Bulletin of the Seismological Society of America, Vol. 98, No. 5, pp. 2349–2363, October 2008, doi: 10.1785/0120080004

Comparison of Site-Effects Estimation Methods Using the Lefkas, Greece, 2003 Earthquake Aftershocks

by Stéphane Drouet, Petros Triantafyllidis, Alexandros Savvaidis, and Nikos Theodulidis

Abstract This study aims at the comparison of different site-effect estimation techniques. We used aftershock records of the 14 August 2003 (M_w 6.2) earthquake that occurred in the western part of Greece next to Lefkas Island. A data set of 15 events recorded at five stations was selected for the period of 20 August 2003–30 September 2003. The moment magnitudes range between 3.3 and 4.2, and the hypocentral distances vary from 5 to 34 km. The site effects are determined using the standard spectral ratio (SSR) method, the horizontal-to-vertical spectral ratio for earthquake data method (the so-called receiver function [RF] method), and an inversion method for simultaneous source, path, and site-effects estimation. These methods are applied to both *P* and *S* waves, using exactly the same time windows in order to compute the spectra. Finally, using geotechnical information available for the city of Lefkas, the experimental site transfer functions at each site are compared to theoretical one-dimensional 1D transfer functions computed using Kennett's reflectivity coefficient method. We show that the SSR method and the inversion method give similar site transfer functions. However, the experimental SSR fits even better with the spectral ratios of the inversion results, which indicates that our reference site is affected by a small site effect. Moreover, the RF method results fit well with the horizontal-to-vertical ratios coming from the inversion results, indicating in this case a nonnegligible amplification on the vertical component. This is the reason why the RF gives only the frequency of amplification but not the amplitude. These conclusions hold for both *P* and *S* waves. Finally, the site effects computed using the whole record or a window including only *S* waves are similar, while the *P* waves results, although showing some similar features with those for *S* waves, give different transfer functions for the sites investigated.

Introduction

Site-effects estimation has been a major issue in engineering seismology for the last 20 years. That is due to the fact that seismic hazard is strongly influenced by site effects because site conditions strongly affect the frequency content and the amplification of the ground motion, and also because most of the populated areas are located in sedimentary basins. Usually, in engineering seismology, site effects are estimated using ambient noise data and/or strong-motion data, or they are modeled using dynamic properties of the geotechnical profile.

Many methods have been proposed for the evaluation of site effects based on accelerogram recordings. The most common one is the standard spectral ratio (SSR) technique, where the spectral ratio of an earthquake record at a sedimentary site to a corresponding one at a nearby rock site is used to calculate the site response (e.g., Borcherdt, 1970). Another technique is the assessment of H/V spectral ratio both from earthquake recordings (the so-called receiver function [RF] method) and ambient noise data, mainly used to derive the fundamental frequency of the investigated site (Nogoshi and Igarashi, 1971; Nakamura, 1989). Additionally, a simultaneous inversion scheme of source, path, and site effects can be applied, using a set of stations that recorded a set of earthquakes (Andrews, 1986). The main advantage of the latter method is that it takes into account attenuation and it provides good site-effects estimation even if all of the stations did not record all of the earthquakes (Field and Jacob, 1995). Several authors compared the results derived from the aforementioned methods (Field and Jacob, 1995; Bonilla *et al.*, 1997; Parolai *et al.* 2004) and found a general agreement between the SSR and the inversion techniques, while the H/V ones seem to give only a reliable estimate of the fundamental frequency but in many cases lower amplitudes.

In this study, site effects are investigated for the city of Lefkas applying the SSR, the RF, and the inversion methods described previously using data from the aftershock activity

of a strong-motion event (M_w 6.2) that hit Lefkas Island on 14 August 2003. Our results are compared to the ones obtained by Triantafyllidis *et al.* (2006), who used the same earthquake data set but the complete record length in order to calculate the experimental transfer functions for the same sites.

The site effects in the city of Lefkas have been thoroughly investigated in the past. For instance, Theodulidis and Tsakalidis (1994) used strong-motion data recorded in the center of the city and geotechnical information in order to compare observed and theoretical (H/V) spectral ratios and theoretical transfer functions. Subsequently, Dimitriu *et al.* (1999, 2001) applied the H/V spectral ratio method on earthquake data recorded at the same site and an adjacent one in order to investigate site effects on sediments, their nonlinearity, and the attenuation κ-factor behavior. Anastasiadis *et al.* (2006) evaluated the subsoil impact in the city of Lefkas using strong ground-motion geotechnical information and numerical calculations.

Data

On 14 August 2003 at 05:14 coordinated universal time (UTC), a strong earthquake with M_w 6.2 occurred close to the island of Lefkas in western Greece (Fig. 1). The earthquake was strongly felt in the Ionian Islands (Cephalonia, Zakynthos, Ithaki, etc.) as well as on the mainland of Greece. The epicenter was located in the Ionian Sea, about 12 km southwest of the town of Lefkas, with epicenter coordinates 38.761° N, 20.600° E at a depth of 8 km (Karakostas *et al.*, 2004).

Within a few days after the mainshock, the Institute of Engineering Seismology and Earthquake Engineering (ITSAK) deployed a temporary network of nine high-resolution digital accelerographs in the broader epicentral area, aiming to investigate strong ground-motion distribution and identify possible site effects (Earthquake Engineering Research Institute [EERI], 2003). Four of these stations were installed in the town of Lefkas (LDD: Forest Directorate, LHS: Hospital, LTH: Town Hall, LMA: Port–Marina) and another one (LMF) near the Monastery of Faneromeni (Fig. 1). The LMF station was considered to be a reference one because it is underlain by limestone. One potential limitation to the use of LMF as reference station is that it is located on a hilly area and maybe subjected to topographic effect. LMF is also located about 2 km west of the town of Lefkas, and differences in travel paths may exist. However, the inversion method we use is less sensitive than the SSR method to differences in travel paths because all

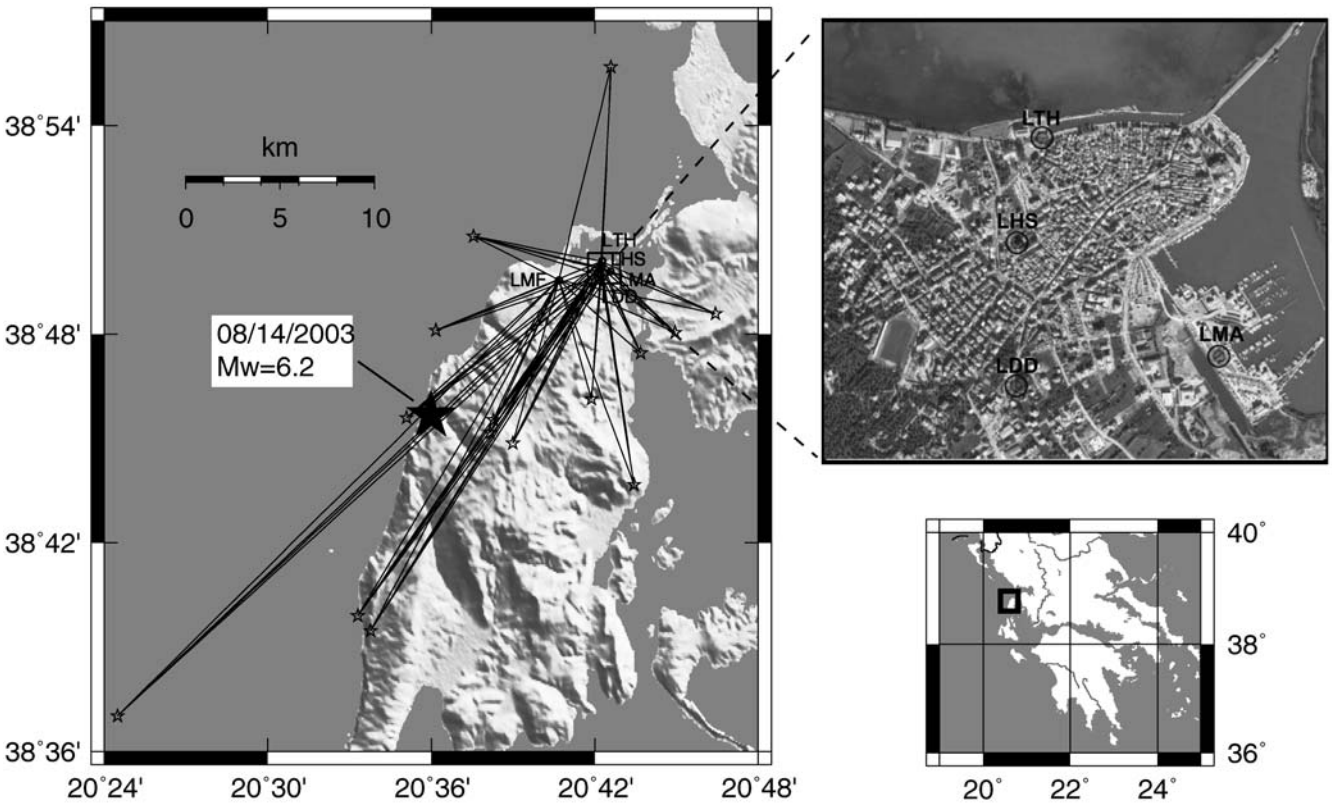

Figure 1. Map of the events (stars), stations (squares), and paths (lines) used in this study. The general localization within Greece is also indicated, as well as a zoom on the city of Lefkas (from GoogleEarth) where four out of the five stations are set up. The localization of the mainshock (14 August 2003, M_w 6.2) is also illustrated.

of the recordings are used together to invert for path properties. The remaining four stations were installed on recent shallow alluvium deposits that underlay almost the whole town of Lefkas (Institute of Geology and Mineral Exploration [IGME], 1963). Shorter duration of the horizontal component, lower amplitudes, and higher frequency content are observed at the recordings of the LMF station with respect to the rest of the stations (Fig. 2). This was an additional indication that LMF serves satisfactorily as a reference site in the SSR method (Triantafyllidis *et al.*, 2006). An average geotechnical profile representative of the central part of the town of Lefkas, around the LHS station, is proposed by Theodulidis and Tsakalidis (1994) and slightly modified by Dimitriu *et al.* (1999) (see the section entitled 1D Theoretical Transfer Function).

From the total temporary network recordings, a data set of 15 events was selected for the period of 20 August 2003–30 September 2003. The seismological parameters provided by Karakostas *et al.* (2004) for these events are given in Table 1. Note that the moment magnitudes are equivalent moment magnitudes (M_w^*) estimated as proposed by Papazachos *et al.* (1997), and they range between 3.3 and 4.2. The earthquakes occurred in an area extending from the southwest to the northern part of the island (Fig. 1). 126 *S* waves and 118 *P* waves horizontal components were used as well as 63 *S* waves and 59 *P* waves vertical components to apply site-effects estimation methods. For the earthquake number 6 (Table 1), the recordings begin shortly after the *P*-wave arrival time.

Methods

Experimental Methods

The data used in the experimental methods and in the inversion were all handled in the same way and submitted to the same process in order to be able to safely compare the results and extract meaningful interpretation. In Triantafyllidis *et al.* (2006), the whole length of the recorded waveforms was used, ranging approximately from 10 to 60 sec. In the present work, we created three data subsets based on the wave type of the records: two of them are made of direct body waves, *P* and *S*, for the sake of comparison with the inversion method, and the other one is made of late-*S* and

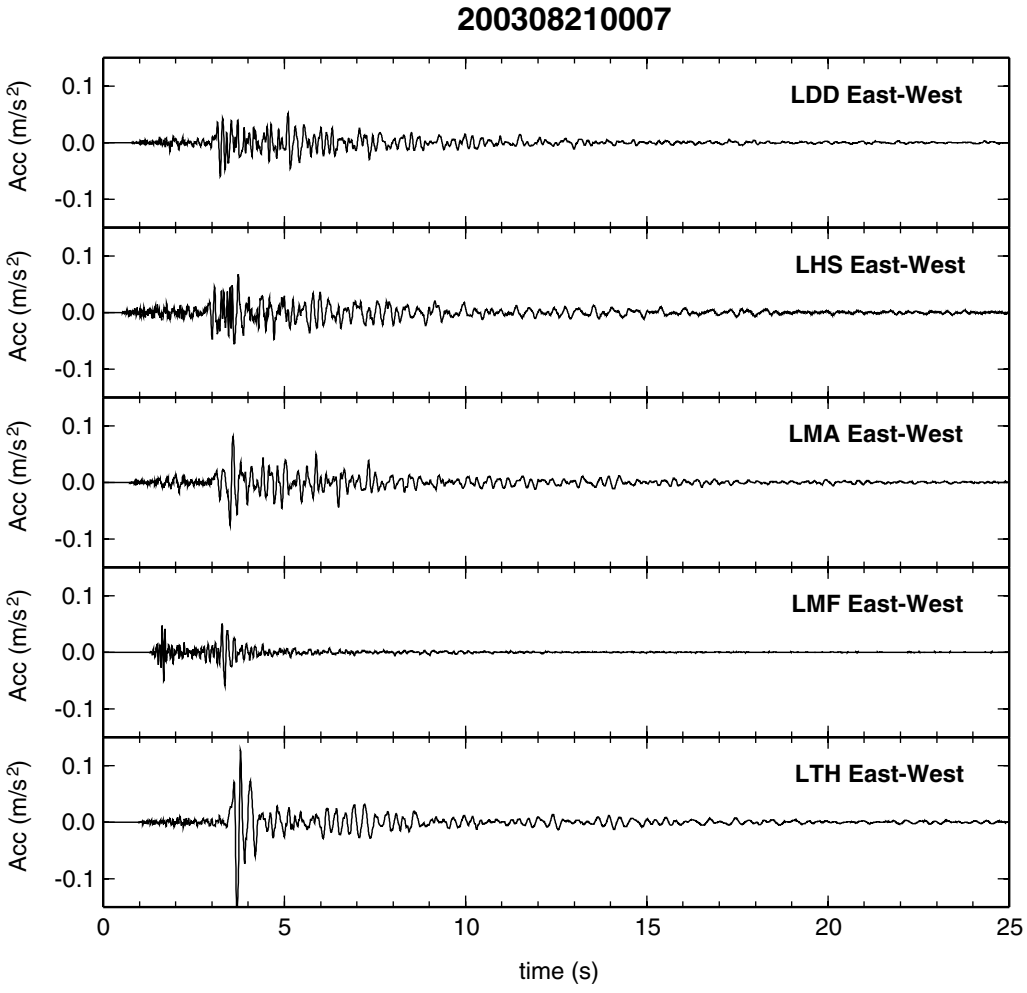

Figure 2. Acceleration time histories for earthquake number 1 (Table 1) recorded at the five stations on the east–west component.

Table 1
Date, Localization (after Karakostas *et al.* [2004]), and Magnitude of the Events Used

Number	Date (dd/mm/yyyy)	Time (UTC)	Latitude (°N)	Longitude (°E)	Depth (km)	M_w (Upatras)*
1	21/08/2003	00:07:39.89	38.802	20.603	10	4.2
2	21/08/2003	05:18:42.74	38.665	20.555	10	4.2
3	21/08/2003	09:58:42.30	38.760	20.585	10	3.9
4	03/09/2003	06:33:25.59	38.847	20.626	26	3.7
5	06/09/2003	06:57:18.46	38.748	20.650	7	3.5
6	06/09/2003	08:59:53.71	38.753	20.636	2	3.5
7	06/09/2003	20:28:20.51	38.759	20.638	34	3.5
8	13/09/2003	04:14:07.80	38.801	20.749	2	3.8
9	13/09/2003	06:44:44.20	38.810	20.774	5	3.6
10	14/09/2003	10:42:00.38	38.791	20.728	7	3.3
11	19/09/2003	12:31:08.01	38.728	20.724	7	3.5
12	23/09/2003	01:23:29.80	38.617	20.408	5	3.7
13	28/09/2003	15:29:26.34	38.928	20.710	10	4.2
14	29/09/2003	12:59:09.43	38.769	20.698	13	3.7
15	30/09/2003	05:56:32.63	38.658	20.563	10	4.1

*Upatras: University of Patras.

surface waves in order to investigate the influence of those waves on site-effects estimation with both the SSR and RF methods. Because of the higher energy content, we focused mainly on the *S*-waves data set, which consisted of waveforms starting from the *S*-wave arrival with a duration of 3 sec. The *P*-waves data set is made up of 4-sec time windows starting before the *P*-wave arrival and ending at the *S*-wave arrival. This fixed window is chosen in order to simplify data processing, and the 4 sec ensure that for each recording the *P*-wave arrival fits within the window. The last data set is composed of waveforms starting right after the *S*-wave window up to the end of the signal, and we conventionally named it as late-*S* and surface waves (LS&surface waves). We did not compute noise spectra because the available noise window was very short in most recordings, but we visually inspected all of the accelerograms and checked that the signal-to-noise ratio was large.

After the splitting of the waveforms in the previously discussed three time windows for all three components (east–west, north–south, vertical), a smoothing algorithm proposed by Konno and Ohmachi (1998) was applied to their Fourier amplitude spectra with smoothing parameter $b = 40$. The site response (or site effects) at each site is (are) estimated through spectral ratios. Therefore, for all of the aforementioned data sets, we applied the SSR technique by dividing the spectra of the horizontal components at each site by the respective spectra of the same earthquake at site LMF. Moreover, we applied the so-called RF technique by taking the spectral ratios between the horizontal and vertical components at each site for each earthquake.

Nonlinear Inversion Method

Following Drouet *et al.* (2008), a parameterized nonlinear iterative inversion method is used in order to separate the source, the path, and site effects from the far-field acceleration spectra. Although the distances are quite short, the small to moderate event sizes and the relatively high frequencies analyzed (0.6–15 Hz) allow us to adopt the far-field hypothesis. Assuming a constant velocity along the path, a frequency- (f_k) dependent quality factor [$Q(f_k) = Q_0 f_k^{\alpha}$], and a constant geometrical decay, the logarithm of the far-field spectra for an earthquake i, at a station j, and for a frequency k can be written as

$$\log_{10}(A_{ijk}) = \log_{10}\left(\frac{2R_{\theta\varphi}M_{0i}}{4\pi\rho\nu^3}\right) + \log_{10}\left(\frac{(2\pi f_k)^2 f_{ci}^2}{f_k^2 + f_{ci}^2}\right) - \gamma\log_{10}(r_{ij}) - \frac{\pi r_{ij} f_k}{\ln(10) Q_0 f_k^{\alpha}\nu} + \log_{10}(S_{jk}), \quad (1)$$

where $R_{\theta\varphi}$ is the average radiation pattern, ρ the density, ν the wave velocity, M_{0i} the seismic moment (in N m), and f_{ci} the corner frequency for the event i. γ is the geometrical attenuation exponent, r_{ij} is the hypocentral distance, Q_0 and α describe the anelastic attenuation, and S_{jk} is the site effect at station j for a frequency k.

Using a set of earthquakes recorded in a number of stations, we can simultaneously invert the source parameters (M_{0i} and f_{ci}), the path parameters (γ, Q_0, and α), as well as the site parameters (S_{jk}).

As shown by Andrews (1986), this kind of inversion has a degree of freedom between the constant terms M_{0i} and S_{jk} that has to be removed. This is done by constraining the site response at each frequency of either one station or an average over a set of stations to be equal to 1, hereafter referred to as reference condition.

For the inversion, a least-squares iterative algorithm proposed by Paige and Saunders (1982) is applied to both the geometrical mean of the horizontal components of *S* waves,

$$H = \sqrt{\frac{EW^2 + NS^2}{2}}, \tag{2}$$

and the vertical component of *P* waves, with the following parameters: $\rho = 2500$ kg/m^3, $v_S = 2000$ m/sec, $v_P = 4000$ m/sec after Dimitriu *et al.* (2001), and $R^P_{\theta\varphi} = 0.33$, $R^S_{\theta\varphi} = 0.55$ after Boore and Boatwright (1984).

Results

Experimental Methods

In Figure 3 the results after the application of the RF technique are presented at each site. The dark solid line indicates the amplification variation of the *S*-waves data set ± one standard deviation (shaded area), while the gray and dark dashed lines show the amplification estimated from the *P*-waves and LS&surface waves data sets, respectively. The gray solid line indicates the results of Triantafyllidis *et al.* (2006), who used the whole record length in their computations. On closer examination, we observe that at all sites for frequencies lower than approximately 1.5 Hz, the spectral amplification level based on the whole record data set is slightly higher than (or similar to) the ones based on *S* waves and LS&surface waves maintaining more or less the same shape. For the frequency range between about 1.5 and 4.5 Hz at all stations (except LMF), we notice a bulge of similar shape for the *S* waves, LS&surface waves, and whole length data sets, whereas the amplification level of the *S*-waves curve is clearly higher than the other two reaching values of 5–6 at stations LDD, LHS, and LMA and about 10 at LTH. At stations LDD and LTH, the LS-surface-waves curve lies outside of the *S*-waves standard deviation area, though preserving the same shape. For frequencies higher than 4.5 Hz, the three amplification curves (*S* waves, LS&surface waves, and whole record) are almost identical both in shape as well as amplitude level. Moreover, at all of the stations and throughout the entire frequency range, the amplitude of the *P*-waves data set is always lower compared to the other three data sets, demonstrating the unsuitability of those waves to be used for site amplification estimation in an engineering point of view. Furthermore, at station LMA, the *S*-waves standard deviation area is quite wide, which is probably due to the relatively small number of data recorded at this site (only five events, see Table 2). One also has to note the larger standard deviation at low frequencies compared to the one at high frequencies, which, in this case, is not due to the number of data. This may be due to the radiation pattern, which affects the low frequencies at larger

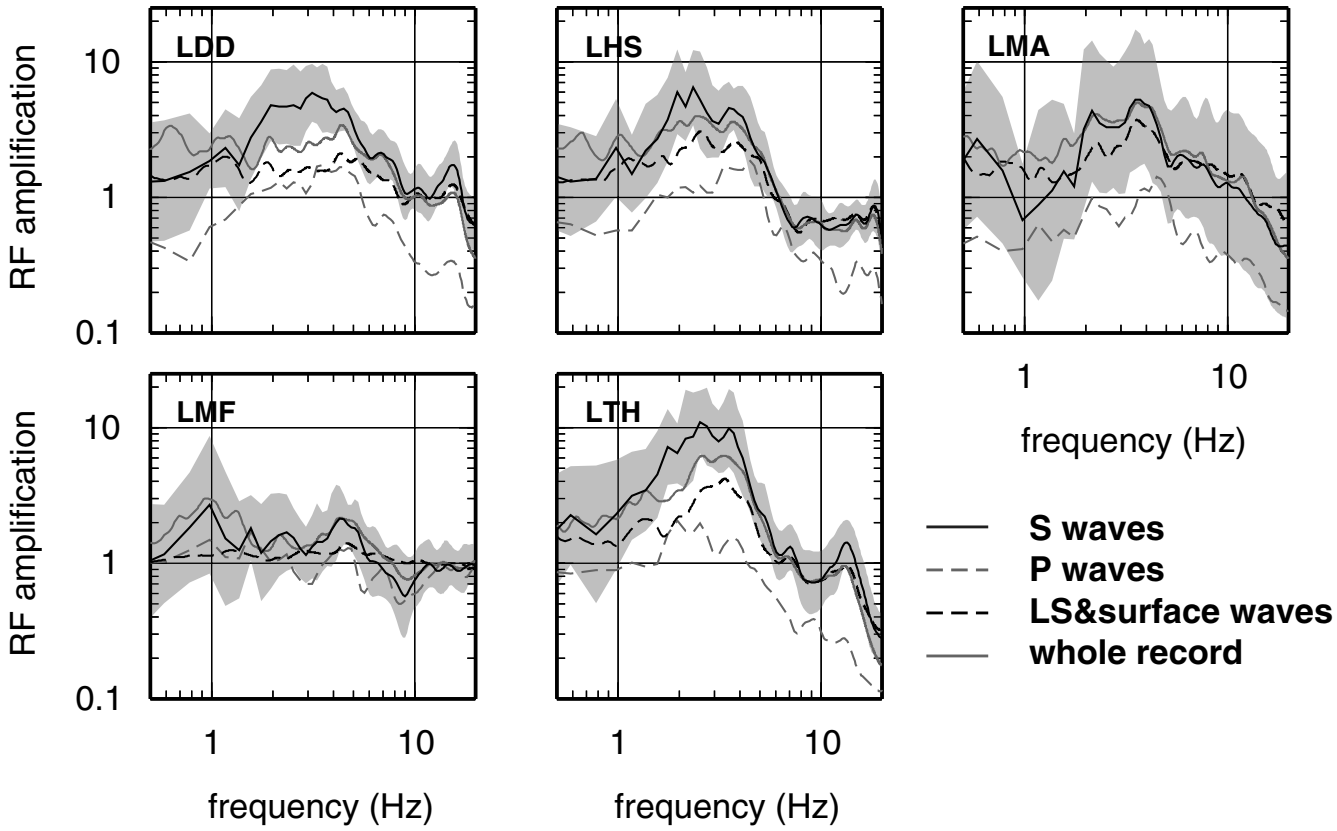

Figure 3. Results of the RF method for the five stations for: *S* waves (mean: solid black lines; mean ± σ: gray shaded area), *P* waves (mean: dashed gray line), LS&surface waves (mean: dashed black line), and for the whole record from Triantafyllidis *et al.* (2006) (mean: solid gray line).

Table 2
Localization of the Stations

Station Name	Latitude (°N)	Longitude (°E)	Altitude (m)	Number of Recodings (3 components), S/P
LDD	38.8281	20.7037	10	13/12
LHS	38.8321	20.7044	10	15/14
LMA	38.8301	20.7097	10	5/5
LMF	38.8260	20.6782	100	15/14
LTH	38.8351	20.7045	10	15/14

distance than the high frequencies because the latter ones attenuate faster.

On the other hand, Figure 4 shows a relatively different image using the SSR method. Apart from the *P*-waves data set, all of the rest (whole record, *S* waves, and LS&surface waves) are rather consistent with each other both in amplitude level and shape at all stations for almost the entire frequency range. A slight difference between the three data sets can be observed at LMA, especially for frequencies above 3 Hz, but all of them vary within the undoubtedly wide *S*-waves standard deviation zone. In addition, as previously mentioned, this might be due to the few events recorded at LMA and, therefore, the small amount of data. At all sites, the *P*-waves spectral ratio hardly lies within the shaded area whereas its amplitude level is strongly underestimated (even three times at LMA) for all frequencies. At stations LTH and LMA, a bulge in the shape of the curves similar to the one seen after the RF technique (Fig. 3) is noticed at frequencies between approximately 1.5 and 6 Hz, reaching amplification factors of 6–8. At LDD and LHS, this bulge is smoother, appearing in a wider frequency range (1–10 Hz) and with an amplification level around 5. The *P*-wave ratios seem to reasonably identify the frequency of maximum amplification.

Nonlinear Inversion

Two independent inversions are performed, one for the horizontal components of *S* waves and the other for the vertical components of *P* waves. These two inversions are applied to the same events except for earthquake number 6 (Table 1), for which *P* waves are not recorded. Moreover, we observed that the *P* waves have less well-defined low frequencies; thus, the bandwidth analyzed for *P* waves was 0.9–15 Hz whereas we used frequencies down to 0.6 Hz for *S* waves. In both cases, two reference conditions are tested:

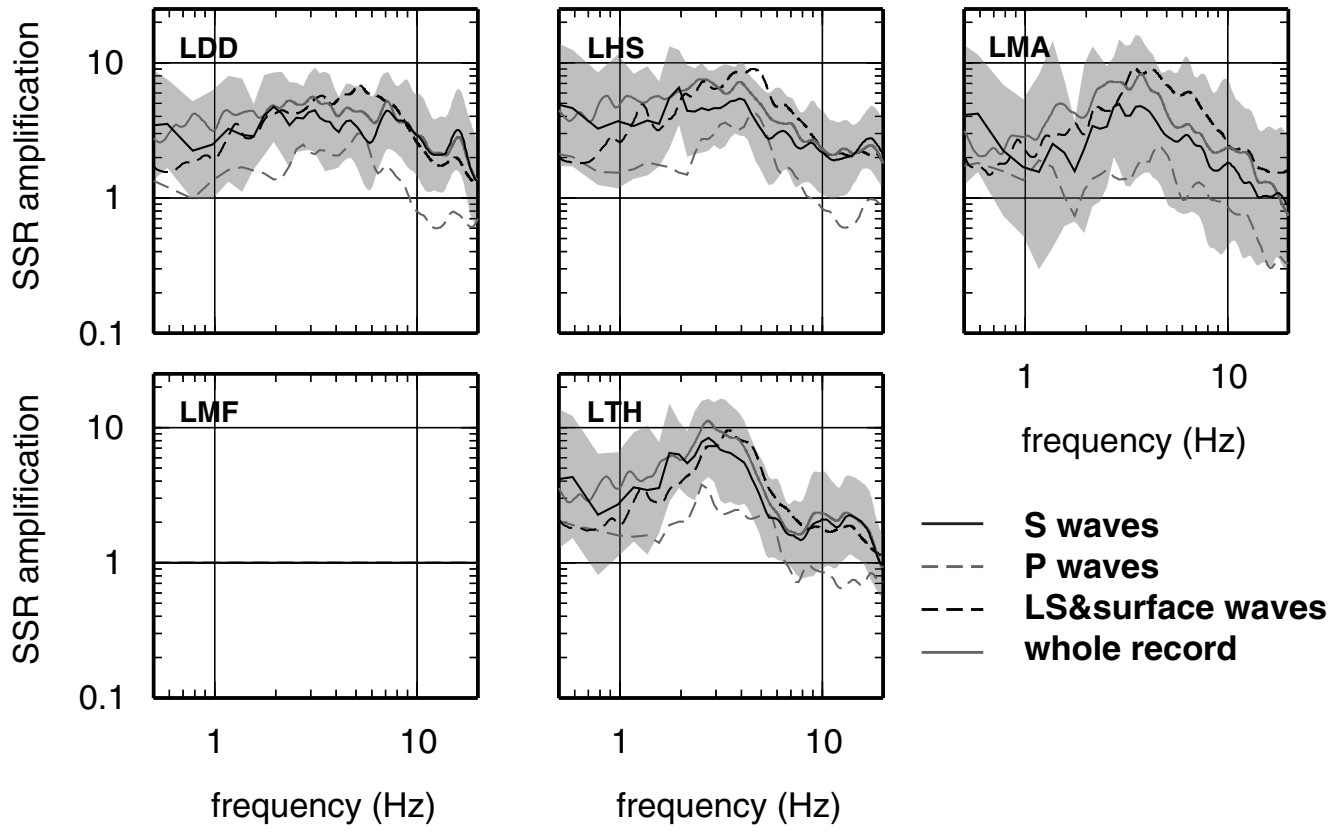

Figure 4. Same as Figure 3 but for the SSR method results.

one by using station LMF as a reference and the other one by using the average site response over the five stations.

As an indication of the quality of the fit, Figure 5 shows for earthquakes number 2 and 9 of Table 1, and for stations LHS and LTH, the observed and modeled far-field spectra for both vertical *P* waves and horizontal *S* waves. Figure 6 depicts the residuals $[\log_{10}(\text{data}) - \log_{10}(\text{model})]$ distribution. This distribution is close to be log-normally distributed, with a standard deviation of 0.17, while the shape of the distribution does not change with frequency. Moreover, the same figure shows that there is no apparent trend in the residuals as a function of distance, magnitude, or frequency.

In Table 3, the attenuation parameters are given for both *S* and *P* waves as well as for the two inversions based on different reference conditions. First, it can be observed that using the mean over all of the stations as a reference leads, for *S* waves, to nonrealistic anelastic attenuation with a decreasing quality factor with frequency ($\alpha \ll 0$), which is opposite to the usual observations in this frequency band. On the other hand, the results for *P* waves are quite stable whichever the reference. As it will be demonstrated in the following section, this is probably due to the fact that the site effects for *P* waves are much smaller than those for *S* waves. Four of the stations are located inside of the city, close to the sea, and are expected to produce high site effects, while station LMF is located on a hill and is probably less affected by site effects. Thus, we place more trust in the results using LMF as a reference. The geometrical exponent is close to 1.3–1.4 depending on the wave type. The quality factor for *P* waves is larger than the quality factor for *S* waves, as it is usually observed. However, the small amount of data with a rather narrow distance range implies that the attenuation parameters are not safely resolved as also shown by the large standard deviation, especially for the quality factor.

The inverted corner frequencies are presented in Figure 7 as a function of the inverted moment magnitudes indicating,

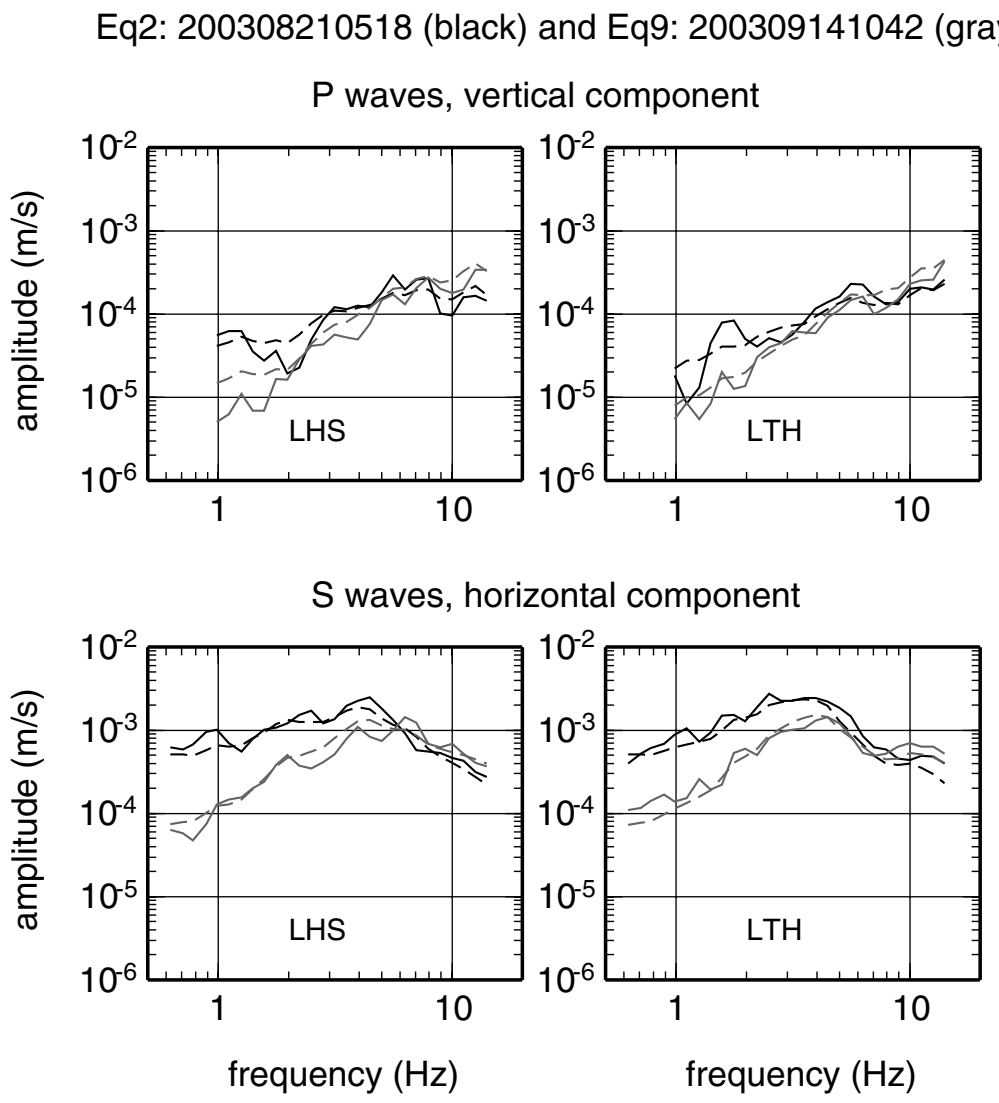

Figure 5. Examples of *P* (top) and *S* (bottom) waves observed (solid lines) and modeled spectra (dashed lines) for the events 2 (black) and 9 (gray) of Table 1 at stations LHS (left) and LTH (right).

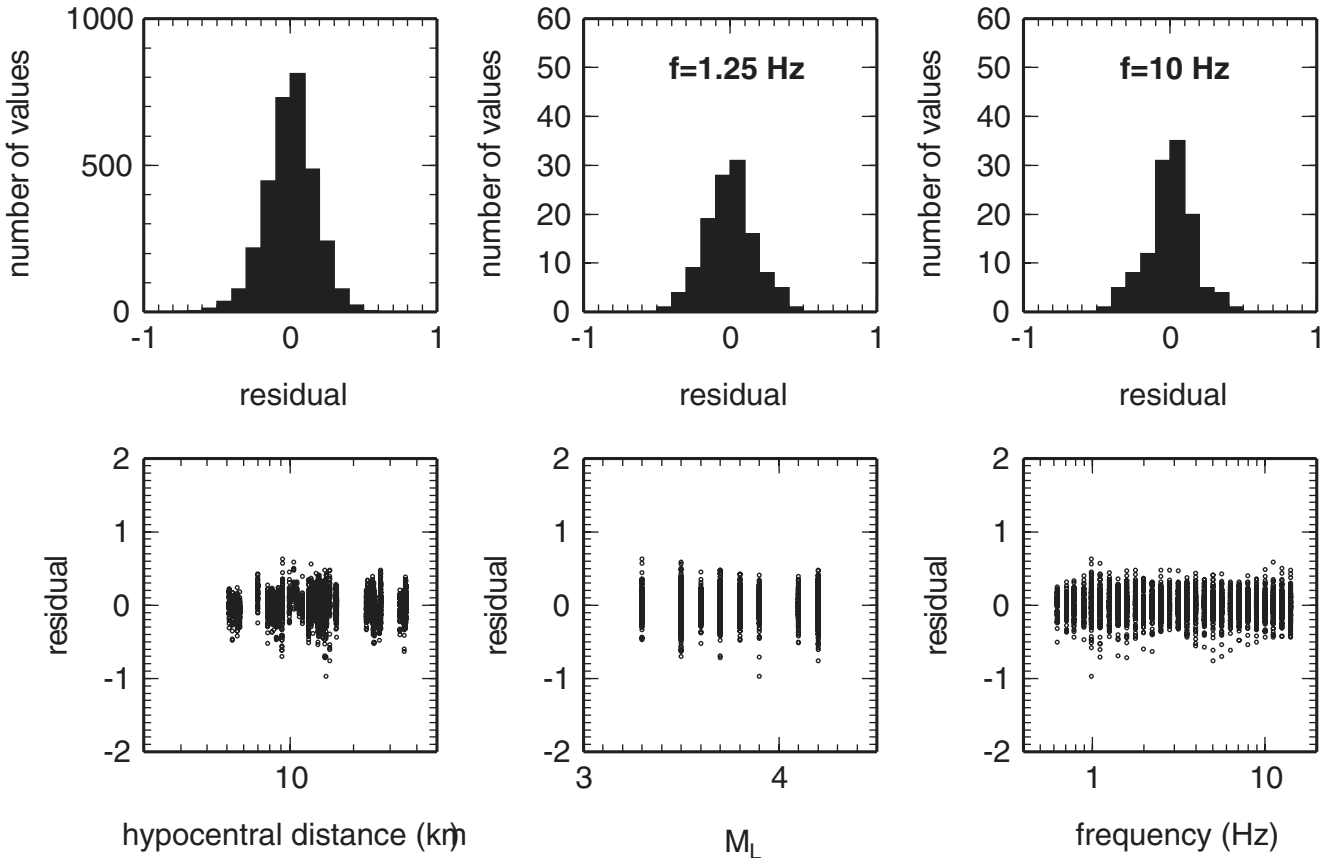

Figure 6. Residuals distribution shown for all of the frequencies (top left) and for 1.25 (middle) and 10 Hz (right). Plots of the residuals as a function of hypocentral distance (bottom left), equivalent moment magnitude (middle), and frequency (right) are also shown.

as expected, that the higher the magnitude, the lower the corner frequency. Moreover, the *P*-waves corner frequencies are in general greater than the *S*-waves corner frequencies with a mean ratio of 1.6, a value close to 1.5 as proposed by Madariaga (1976). The moment magnitudes determined from the seismic moments are in good agreement between *P* and *S* waves and are close to the equivalent moment magnitudes determined by the University of Patras, as shown in Figure 7.

Those inversions also provide the site effects for the horizontal component of *S* waves and the vertical component of *P* waves. In order to compute the vertical response for *S* waves and the horizontal response for *P* waves, we subtract the source and path terms (the first four terms on right-hand side of equation 1) from the data, assuming that they are the same for both horizontal and vertical components. For this purpose, we use the previously determined source and path parameters and invert only for the site parameters. This last inversion is linear and thus no iteration is required. We finally have horizontal and vertical site transfer functions for both *P* and *S* waves. Figure 8 manifests the horizontal and vertical inverted transfer functions ± one standard deviation for *S* and *P* waves using LMF as a reference. In order to show the influence of the reference condition, we also plot the vertical transfer functions for *P* waves and the horizontal transfer functions for *S* waves, using the average over all of the stations as a reference. The influence of the reference is essential for *S* waves and consists in a shift of the amplitude of the transfer functions. Indeed, four out of the five stations are subjected to large site effects (nonflat transfer functions [TF]), especially LHS, LMA, and LTH; thus, the average amplification cannot be equal to 1 and consequently the average reference condition cannot be valid. Therefore, the results using only LMF in the reference condition are more reliable. For *P* waves, the results are less dependent on the reference condition because smaller amplifications are observed at the sediment sites.

Table 3
Inverted Attenuation Parameters for *S* and *P* Waves
(Mean ± One Standard Deviation)

	Reference LMF	Reference All
γ^s	1.40 ± 0.05	1.32 ± 0.04
Q_0^S	433 ± 314	632 ± 398
α^S	-0.04 ± 0.22	-0.37 ± 0.21
γ^P	1.32 ± 0.05	1.32 ± 0.05
Q_0^P	447 ± 503	374 ± 411
α^P	0.60 ± 0.38	0.53 ± 0.37

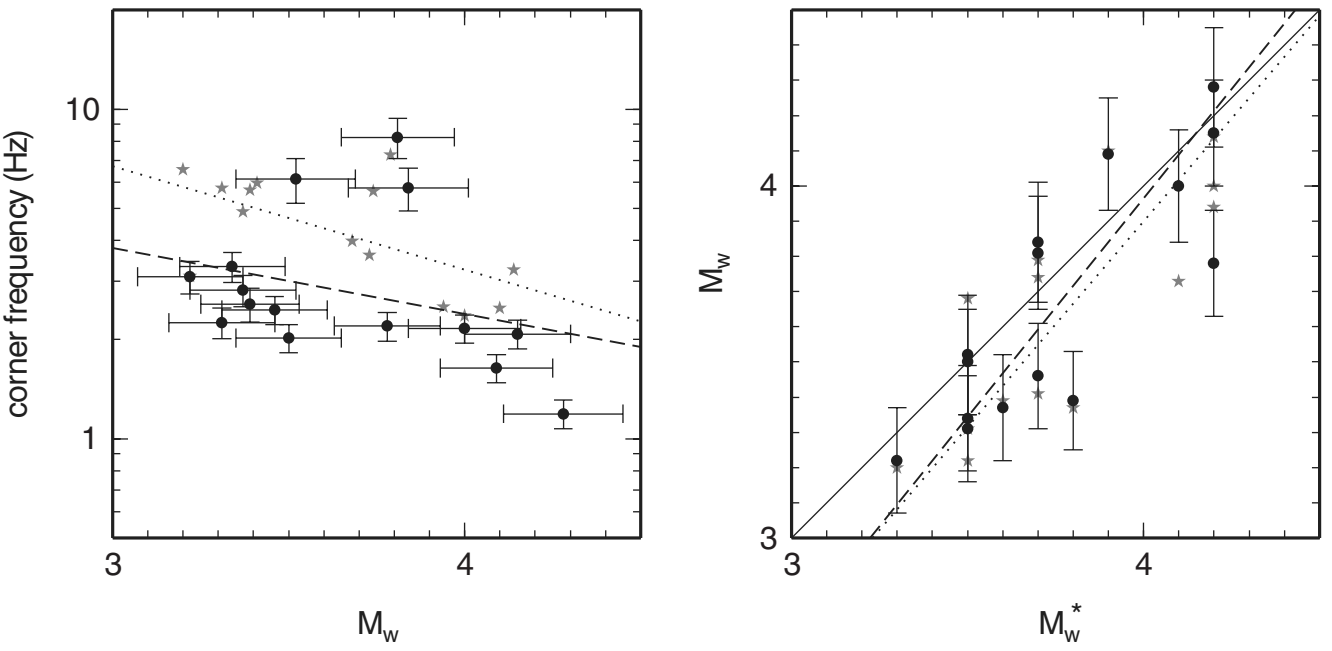

Figure 7. Plot of the inverted corner frequencies as a function of the inverted moment magnitudes (left) for *P* (gray stars) and *S* (black circles) waves. Plot of the inverted moment magnitudes as a function of the equivalent moment magnitudes (right) given in Table 1. The dashed and dotted lines are the regression of the *S*-waves and *P*-waves results, respectively.

1D Theoretical Transfer function

The theoretical transfer function is defined as the free-surface ground motion at the top of the layered site divided by the free-surface ground motion of the bedrock outcrop. To compute it, an adapted implementation developed at Laboratoire de Géophysique Interne et Tectonophysique/ Institut de Recherches Interdisciplinaires de Géologie et de Mécanique, Grenoble, of Kennett's reflectivity coefficient method (Kennett and Kerry, 1979) was used. The method operates in the frequency domain and uses as input any type of body waves (*P*, *SV*, *SH*), incident at an arbitrary angle to the one-dimensional (1D) model of the soil structure studied (see Table 4). The output comprises the complex or real transfer function of a site on the 1D model free surface either relative to any interface within the deposit or relative to the free bedrock surface.

Figure 9 compares the modeled and inverted TF for the horizontal and vertical components of *S* wave and the corresponding horizontal-to-vertical ratios at station LHS. We used a 20° of incidence to account for the proximity of the source and that ray paths are not perfectly vertical. However, the incidence angle has a limited influence on the amplification values but not on the shape of the curves. The left panel of Figure 9 shows the *SV*-wave horizontal theoretical TF for a 20°-incidence angle, the *SH*-wave horizontal theoretical TF for vertical incidence, as well as the inverted horizontal TF for *S* waves. The middle panel gives the *SV* wave vertical theoretical TF for a 20°-incidence angle together with the inverted vertical TF for *S* waves. The right panel depicts the horizontal-to-vertical ratios of the *SV*-wave TFs and of the inverted TFs. The shapes of the transfer functions, both horizontal and vertical, as well as the H/V ratios, are in relatively good agreement for the first peak of amplification but the fundamental frequency observed on the theoretical ones is lower than on the observed ones. Therefore, we decided to modify the model given in Table 4 by increasing the *S*-wave velocity of the uppermost layer from 100 to 150 m/sec. The corresponding results are the dashed (for *SV* wave) and dotted-dashed (for *SH* wave) lines in Figure 9. After this modification, the peaks of amplification match for the horizontal transfer functions; however, the horizontal-to-vertical spectral ratio based on the new model shows a poorer fit than that based on the original model, as long as shape of the vertical transfer function does not change.

Experimental versus Inverted Spectral Ratios

In order to further compare the methods, we computed the spectral ratios from the inverted transfer functions. For each site, the inverted horizontal transfer function is divided by either the inverted horizontal transfer function at the reference site (inverted SSR) or by the inverted vertical transfer function at the same site (inverted RF).

Figures 10 and 11 compare the experimental and inverted RF and the experimental and inverted SSR results, respectively, for both *P* and *S* waves. The gray dotted curve and the shaded area show the experimental ratios ± one standard deviation, whereas the solid black and gray curves depict the ratios from the inversion results using LMF and the average

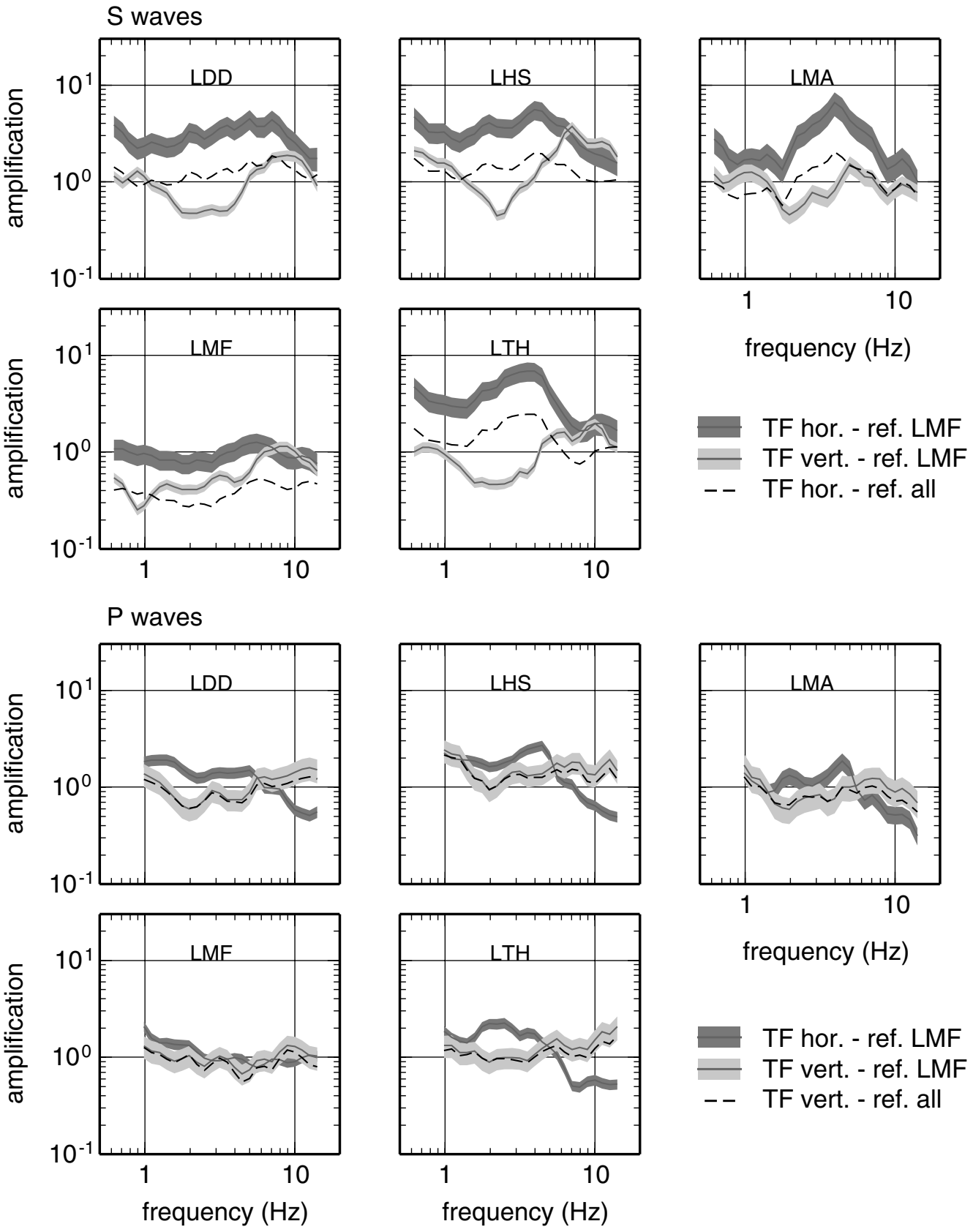

Figure 8. Inverted horizontal (dark greyed area) and vertical (light grayed area) site transfer functions (TF) ± one standard deviation for *S* (top) and *P* (bottom) waves using LMF as a reference. The dashed lines correspond to the horizontal TF for *S* waves and vertical TF for *P* waves, using the average over all of the stations as a reference.

Table 4
Lefkas LHS Site Structure Used in Linear One-Dimensional Modeling
(Adapted from Theodulidis and Tsakalidis [1994])

	H (m)	Density (kg/m^3)	V_s (m/sec)	Q_s	V_p (m/sec)	Q_p
Layer 1	8	1900	100	17	170	30
Bedrock	∞	2200	600	50	1080	120

over all of the stations as a reference, respectively. As long as the influence of the reference condition on the inverted transfer functions consists only in a shift of the amplitudes, the inverted spectral ratios are almost unchanged whichever the reference.

One can observe that due to the amplifications observed either at the reference site or on the vertical component at all the stations, the ratios (both RF and SSR) are different from the transfer functions (compare Figs. 10 and 11 and Figure 8). On the other hand, one can note the good agreement between experimental and inverted RF or SSR as shown in Figures 10 and 11.

Discussion and Conclusions

Three methods for estimating the site effects for five stations in the city of Lefkas have been compared in this study: the standard spectral ratio (SSR) method, the so-called receiver function (RF) method, and a parametrized inversion for source, path, and site effects. The results have also been compared to a 1D theoretical modeling using Kennett's reflectivity coefficient method.

The inversion method has been carried out for both *P* and *S* waves, giving reliable results for path attenuation and source parameters. The geometrical spreading exponent and the moment magnitudes are almost the same for *P* and *S* waves, the quality factor for *P* waves is higher than that for *S* waves, as expected, and the *P*-waves corner frequencies are on average 1.6 times greater than *S*-waves corner frequencies (close to the 1.5 value given by Madariaga [1976]). Even with rather small distance and magnitude ranges, the residuals are log-normally distributed and no apparent bias is observed as a function of distance, magnitude, or frequency.

The site responses obtained for *S* waves, using all three methods at the Lefkas stations, are in agreement with previous studies using the RF method (Dimitriu *et al.*, 1999; Triantafyllidis *et al.*, 2006). An amplification is observed for all of the stations within the city with amplitudes of 4–10 at frequencies between 2 and 5 Hz. The SSR and RF methods results using the whole record are close to those obtained using a narrow window containing direct *S* waves. Parolai *et al.* (2004) also found little dependence on the window length. On the other hand, using the part of the record directly after the *S* waves that we conventionally call LS&surface waves, leads to slightly different amplification. Additionally, the results obtained with *P* waves share similar features with those for *S* waves as long as the frequencies of maximum amplification are almost the same but have considerably lower amplitudes.

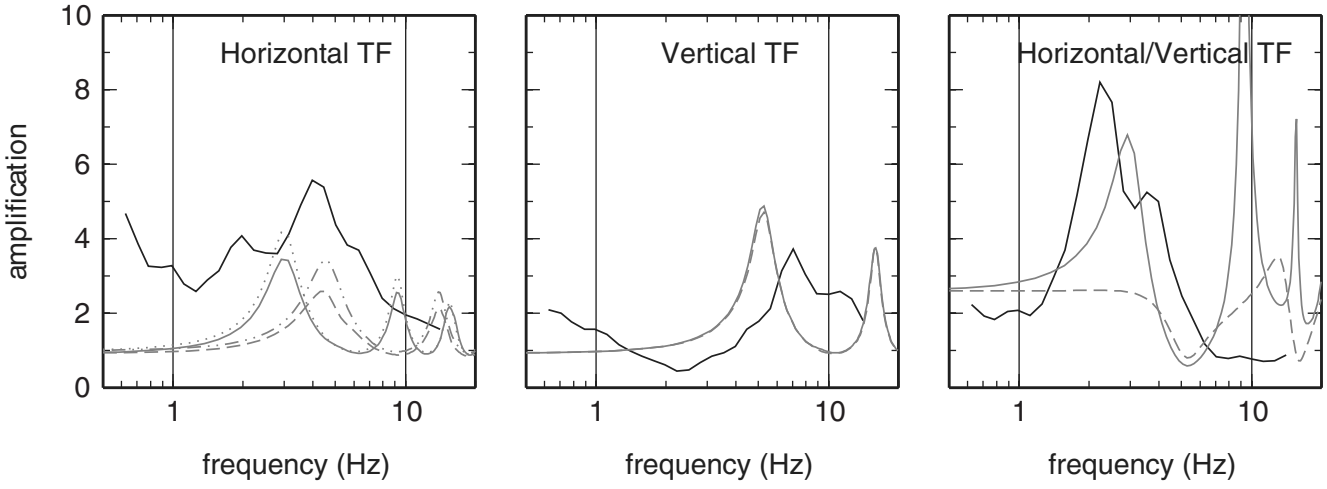

Figure 9. Comparison of theoretical and inverted transfer functions at station LHS. Left: *SV*-wave horizontal theoretical TF for a 20° incidence angle (solid and dashed gray lines) and *SH*-wave horizontal theoretical TF for vertical incidence (dotted and dashed-dotted gray lines) using two different layered models, along with inverted horizontal TF for *S* waves (solid black line). Middle: *SV*-wave vertical theoretical TF for a 20° incidence angle (solid and dashed gray lines) using two different layered models, along with inverted vertical TF for *S* waves (solid black line). Right: ratio between horizontal and vertical components for *SV*-wave theoretical TFs (solid and dashed gray lines) using two different layered models, along with *S*-wave inverted TFs (solid black line).

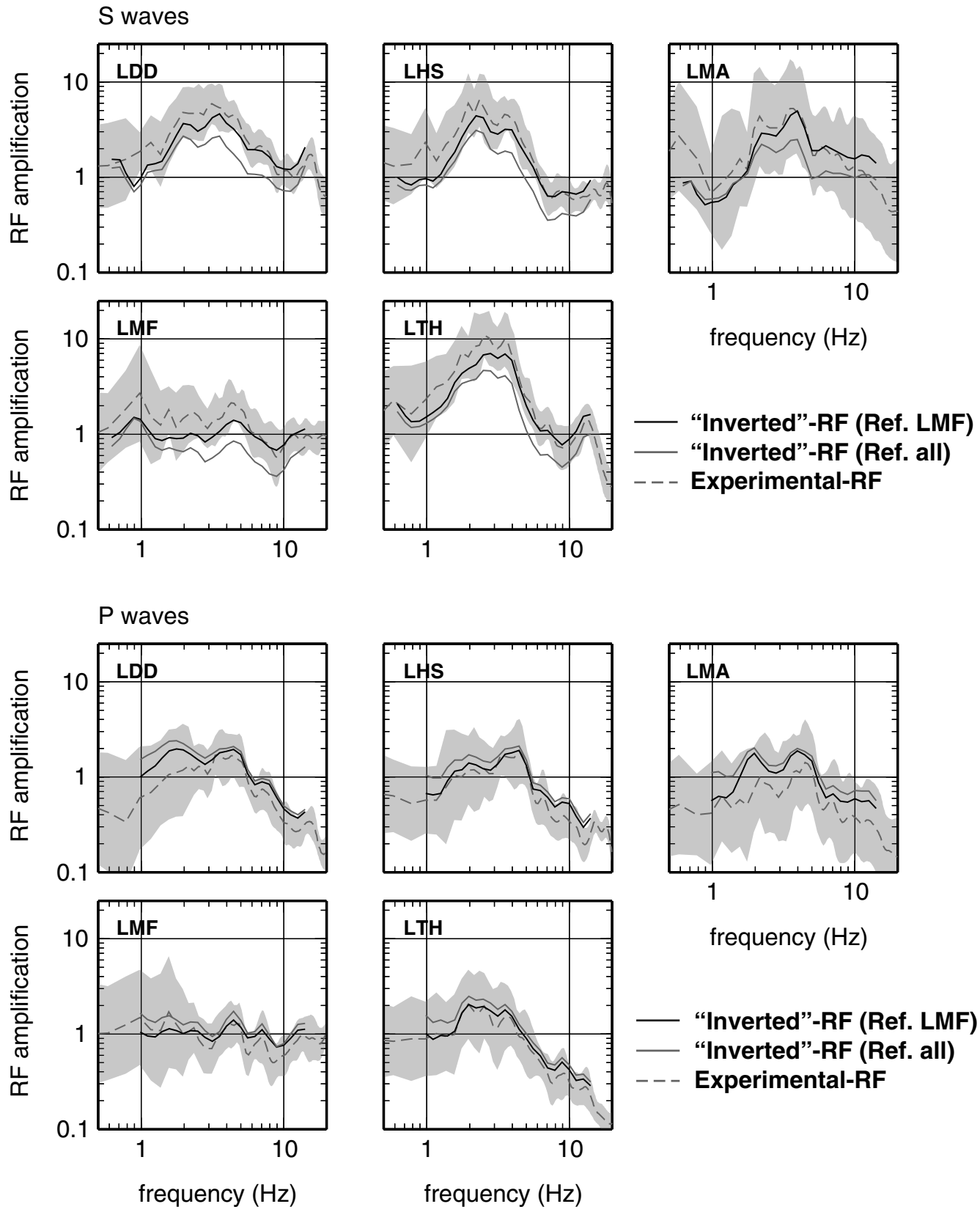

Figure 10. Comparison of empirical RF (mean $\pm \sigma$: dashed gray lines and shaded areas) with inverted RF, using LMF as a reference (solid black lines), and the average over all of the stations as a reference (solid gray lines), for *P* and *S* waves.

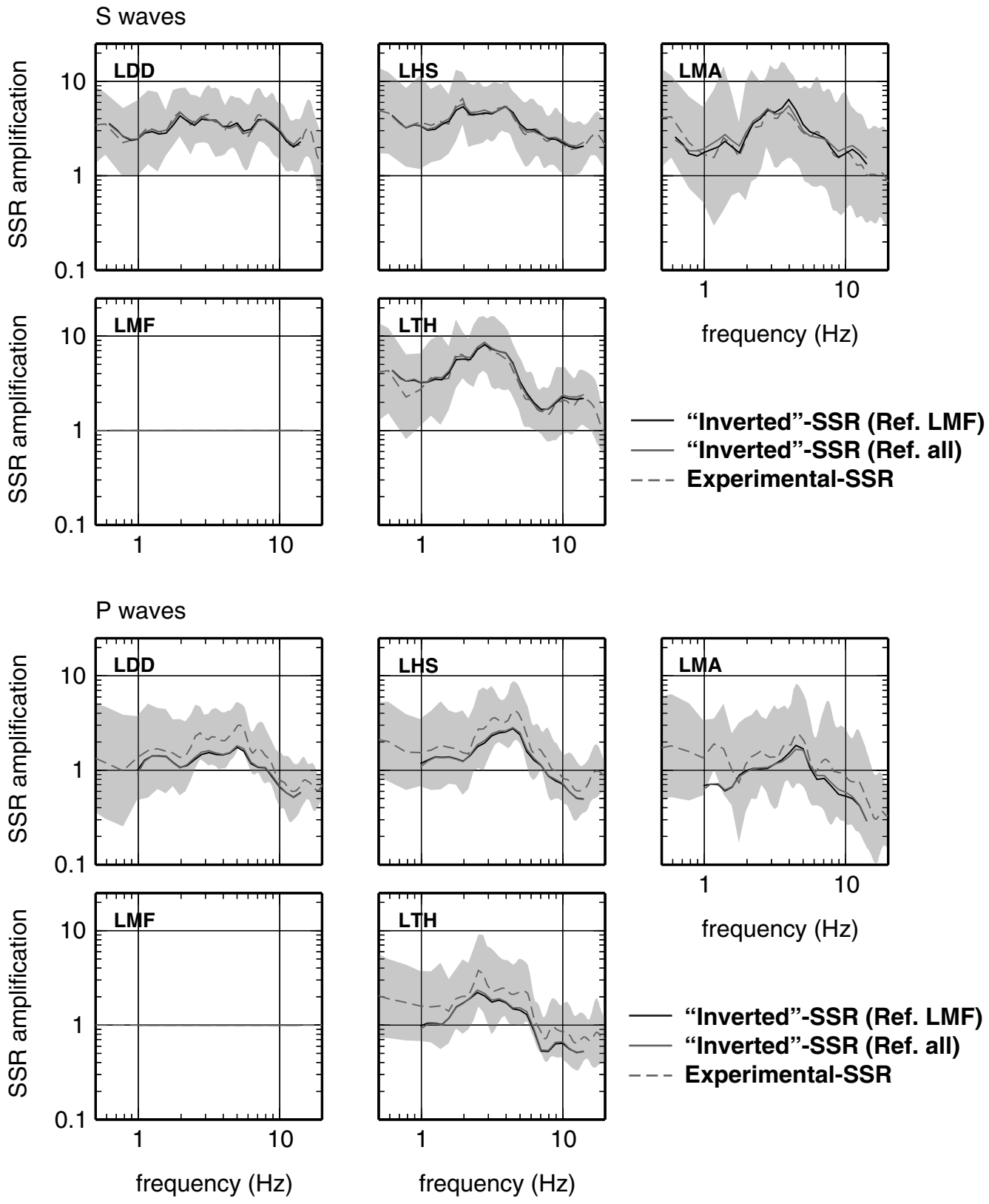

Figure 11. Same as Figure 10 but for comparison of empirical SSR and inverted SSR.

We also compare the site transfer functions for *S* waves obtained from the inversion with those computed using a 1D theoretical modeling. The general shape of the curves is consistent, but we noted that the frequency of amplification differs faintly between the methods. As long as the model used is an average for the city of Lefkas, we tried to change the *S*-wave velocity of the uppermost layer. The consequence is a shift of the frequency of amplification for the horizontal component. However, the vertical component remains almost unchanged and thus the horizontal-to-vertical spectral ratios do not fit anymore.

Several authors compared the site effects estimated from the generalized inversion method and the site effects estimated from other spectral ratios methods (Field and Jacob, 1995; Bonilla *et al.* 1997; Parolai *et al.*, 2004). These authors agree that the inversion and the SSR method give similar results, while the RF method, both for noise and *S* waves, gives the same frequencies of amplification as the other methods but with, in general, lower amplitudes. Nevertheless, they assume that the results are directly comparable and that all of the methods provide the transfer function of the site of interest. These authors explain the difference between the inversion and SSR or RF methods as a result of amplification at the reference site or on the vertical component, respectively, but without clear illustration. In this study, we computed the site transfer functions for both *P* and *S* waves, and for the horizontal and vertical components at all of the sites. We computed the SSR and the horizontal-to-vertical spectral ratios from the inverted site transfer functions. The results seem to be in excellent agreement with the experimental ratios. The reference station shows little, although some, amplification, while the vertical components at all of the stations show some nonnegligible amplification. Those results thus clearly confirm that the SSR method will give a better estimation of the site effect than the H/V because the reference station is less affected by site effects than the vertical components.

We have also shown that the site transfer functions for *P* and *S* waves are different. This is a controversial issue, because Parolai *et al.* (2004) found that site responses from *P* waves are comparable to those from *S* waves, while Field and Jacob (1995) found the opposite result. In this article, the transfer functions from *P* waves may share similar features with those for *S* waves, but with considerably lower amplitudes.

Data and Resources

Data are the property of ITSAK and are available upon request. All of the plots were made using the Generic Mapping Tools version 4.2.1 (http://gmt.soest.hawaii.edu/; Wessel and Smith, 1998).

Acknowledgments

We would like to thank the two reviewers, P. Suhadolc and J. J. Bommer, for their comments that greatly helped to improve this manuscript, and D. M. Boore for his very helpful and constructive remarks on this work. We are also grateful to our ITSAK colleagues for operating the aftershock network and V. Karakostas for providing seismological information of the used events. This work was funded by the European Commission through the Marie Curie Actions—Transfer of Knowledge/Development (TOK/DEV) program. (Contract Number MTKD-CT-2005-029627; Acronym: ITSAK-GR).

References

Anastasiadis, A., B. Margaris, N. Klimis, K. Makra, and K. Pitilakis (2006). The Lefkas earthquake ($M = 6.2$, Aug. 14th, 2003): strong ground motion and evaluation of the subsoil's impact, in *5th Hellenic Conference of Geotechnical and Geoenvironmental Engineering*, Xanthi, Greece, 31 May–2 June 2006, paper 4-12 (in Greek).

Andrews, D. J. (1986). Objective determination of source parameters and similarity of earthquakes of different size, *Earthquake Source Mechanics*, S. Das, J. Boatwright and C. H. Scholz (Editors), American Geophysical Monograph, **37**, 259–267.

Bonilla, L. F., J. H. Steidl, G. T. Lindley, A. G. Tumarkin, and R. J. Archuleta (1997). Site amplification in the San Fernando Valley, California: variability of site-effect estimation using the *S*-wave, coda, and H/V methods, *Bull. Seismol. Soc. Am.* **87,** no. 3, 710–730.

Boore, D., and J. Boatwright (1984). Average body-wave radiation coefficients, *Bull. Seismol. Soc. Am.* **74,** no. 5, 1615–1621.

Borcherdt, R. D. (1970). Effects of local geology on ground motion near San Francisco Bay, *Bull. Seismol. Soc. Am.* **60,** no. 1, 29–61.

Dimitriu, P., I. Kalogeras, and N. Theodulidis (1999). Evidence of nonlinear site response in horizontal-to-vertical spectral ratio from near-field earthquakes, *Soil Dyn. Earthquake Eng.* **18,** 423–435.

Dimitriu, P., N. Theodulidis, P. Hatzidimitriou, and A. Anastasiadis (2001). Sediment non-linearity and attenuation of seismic waves: a study of accelerograms from Lefkas, western Greece, *Soil Dyn. Earthquake Eng.* **21,** 63–73.

Drouet, S., S. Chevrot, F. Cotton, and A. Souriau (2008). Simultaneous inversion of source spectra, attenuation parameters and site responses: application to the data of the French Accelerometric Network, *Bull. Seismol. Soc. Am.* **98,** no. 1, 198–219.

Earthquake Engineering Research Institute (EERI) (2003). EERI Special Earthquake Report, Institute of Engineering Seismology and Earthquake Engineering, National Technical University of Athens, and University of Athens, November 2003, 1–12.

Field, H., and K. H. Jacob (1995). A comparison and test of various site-response estimation techniques, including three that are not reference-site dependent, *Bull. Seismol. Soc. Am* **85,** no. 4, 1127–1143.

Institute of Geology and Mineral Exploration (IGME) (1963). Geological map of Lefkas, Edition of the Institute of Geology and Mineral Exploration, Athens, Greece.

Karakostas, V. G., E. E. Papadimitriou, and C. B. Papazachos (2004). Properties of the 2003 Lefkada, Ionian Islands, Greece, earthquake seismic sequence and seismicity triggering, *Bull. Seismol. Soc. Am.* **94,** no. 5, 1976–1981.

Kennett, B. L. N., and N. J. Kerry (1979). Seismic waves in a stratified half space, *Geophys. J. Int.* **57,** no. 3, 557–583.

Konno, K., and T. Ohmachi (1998). Ground-motion characteristics estimated from spectral ratio between horizontal and vertical components of microtremor, *Bull. Seismol. Soc. Am.* **88,** 228–241.

Madariaga, R. (1976). Dynamics of an expending circular fault, *Bull. Seismol. Soc. Am.* **66,** no. 3, 639–666.

Nakamura, Y. (1989). A method for dynamic characteristics estimation of subsurface using microtremor on the ground surface, *QR Railw. Tech. Res. Inst.* **30,** 25–33.

Nogoshi, M., and T. Igarashi (1971). On the amplitude characteristics of microtremor (part 2), *J. Seism. Soc. Jpn.* **24,** 26–40.

Paige, C. C., and M. A. Saunders (1982). LSQR: an algorithm for sparse linear equations and sparse least squares, *ACM Trans. Math. Soft* **8,** 43–71.

Papazachos, B. C., A. A. Kiratzi, and B. G. Karacostas (1997). Toward a homogeneous moment-magnitude determination for earthquakes in Greece and the surrounding area, *Bull. Seismol. Soc. Am.* **87,** no. 2, 474–483.

Parolai, S., D. Bindi, M. Baumbach, H. Grosser, C. Milkereit, S. Karakisa, and S. Zünbül (2004). Comparison of different site response estimation techniques using aftershocks of the 1999 Izmit earthquake, *Bull. Seismol. Soc. Am.* **94,** no. 3, 1096–1108.

Theodulidis, N., and K. Tsakalidis (1994). Site effects on strong ground motion over simple geology structure: the cases of Lefkas and Argostoli (Greece), in *Proceedings of the XXIV General Assembly of the European Seismological Commission, III*, 1640–1649.

Triantafyllidis, P., N. Theodulidis, A. Savvaidis, and P. Dimitriu (2006). Site effects estimation using earthquake and ambient noise data: the case of Lefkas town, in *First European Conference on Earthquake Engineering and Seismology*, Geneva, Switzerland, 3–8 September 2006, paper 1249.

Wessel, P., and W. H. F. Smith (1998). New, improved version of the Generic Mapping Tools released, *Eos Trans. AGU* **79,** 579.

Institute of Engineering Seismology and Earthquake Engineering (ITSAK)
46 Georgikis Scholis, Thessaloniki
P.O. Box 53, 55102 Finikas
Thessaloniki, Greece
(S.D., A.S., N.T.)

Aristotle University
Computer Science Department
P.O. Box 114, 54124
Thessaloniki, Greece
(P.T.)

Manuscript received 15 November 2007